RESEARCH　　　　　　　　　　　　　　　　　　　　　　　　　　　　　**Open Access**

PROTAC-mediated vimentin degradation promotes terminal erythroid differentiation of pluripotent stem cells

Hao Yan[1†], Ruge Zang[1*†], Tiantian Cui[1], Yiming Liu[1], Biao Zhang[1], Lingpin Zhao[1], Hongyu Li[1], Juannian Zhou[1], Haiyang Wang[1], Quan Zeng[1], Lei Xu[1], Yuqi Zhou[1], Xuetao Pei[1], Jiafei Xi[1*] and Wen Yue[1*]

Abstract

Background Human pluripotent stem cells (hPSCs), including human embryonic stem cells (hESCs) and induced pluripotent stem cells (hiPSCs), can undergo erythroid differentiation, offering a potentially invaluable resource for generating large quantities of erythroid cells. However, the majority of erythrocytes derived from hPSCs fail to enucleate compared with those derived from cord blood progenitors, with an unknown molecular basis for this difference. The expression of vimentin (VIM) is retained in erythroid cells differentiated from hPSCs but is absent in mature erythrocytes. Further exploration is required to ascertain whether VIM plays a critical role in enucleation and to elucidate the underlying mechanisms.

Methods In this study, we established a hESC line with reversible vimentin degradation (dTAG-VIM-H9) using the proteolysis-targeting chimera (PROTAC) platform. Various time-course studies, including erythropoiesis from CD34+ human umbilical cord blood and three-dimensional (3D) organoid culture from hESCs, morphological analysis, quantitative real-time PCR (qRT-PCR), western blotting, flow cytometry, karyotyping, cytospin, Benzidine-Giemsa staining, immunofluorescence assay, and high-speed cell imaging analysis, were conducted to examine and compare the characteristics of hESCs and those with vimentin degradation, as well as their differentiated erythroid cells.

Results Vimentin expression diminished during normal erythropoiesis in CD34+ cord blood cells, whereas it persisted in erythroid cells differentiated from hESC. Depletion of vimentin using the degradation tag (dTAG) system promotes erythroid enucleation in dTAG-VIM-H9 cells. Nuclear polarization of erythroblasts is elevated by elimination of vimentin.

Conclusions VIM disappear during the normal maturation of erythroid cells, whereas they are retained in erythroid cells differentiated from hPSCs. We found that retention of vimentin during erythropoiesis impairs erythroid

---

†Hao Yan and Ruge Zang contributed equally to this work.

*Correspondence:
Ruge Zang
rugezang@163.com
Jiafei Xi
xi_jiafei@126.com
Wen Yue
yuewen@bmi.ac.cn

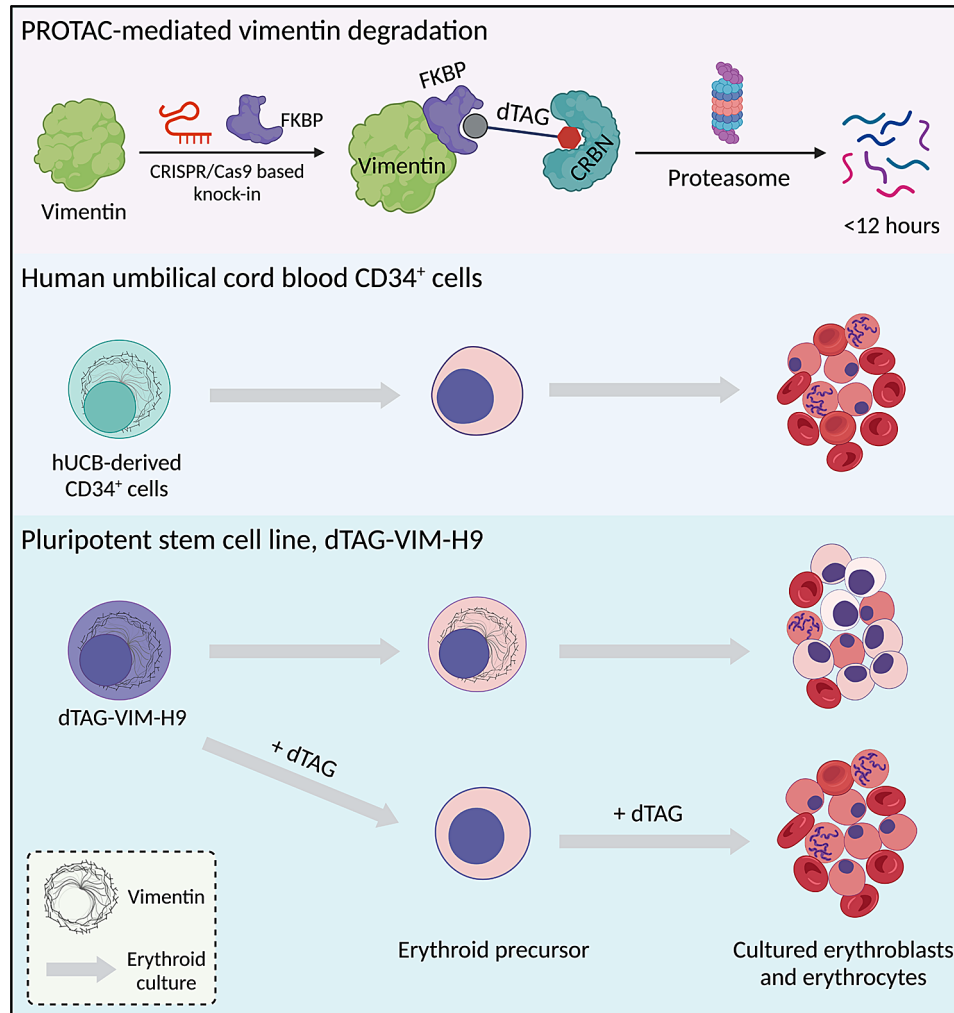Full list of author information is available at the end of the article

enucleation from hPSCs. Using the PROTAC platform, we validated that vimentin degradation by dTAG accelerates the enucleation rate in dTAG-VIM-H9 cells by enhancing nuclear polarization.

Graphical Abstract

Introduction

The in vitro generation of red blood cells (RBCs) holds great promise for transfusion medicine and cell-based therapies given the escalating demand for donated blood and the declining number of blood donors [1, 2]. Research on the generation of cultured human RBCs has been ongoing since the late 1980s [3–5]. Although hematopoietic stem and progenitor cells (HSPCs) derived from bone marrow, cord blood (CB), and adult peripheral blood can give rise to erythrocytes [6], this donor-dependent collection method is constrained by a limited number of cell sources and immune risks associated with variable CD34+ HSPC production heterogeneity. The emergence of human pluripotent stem cells (hPSCs), owing to their self-renewal capacity and differentiation potential, presents a significant opportunity to address these limitations in obtaining erythrocytes [7, 8]. hPSCs include human embryonic stem cells (hESCs) and induced pluripotent stem cells (hiPSCs). Numerous endeavors are underway to obtain RBCs derived from hPSCs with the aim of diminishing reliance on blood transfusions [9–12].

The generation of circulating RBCs is the outcome of erythropoiesis, a complex multistep process involving the proliferation and differentiation of HSPCs into mature enucleated RBCs [13]. Erythropoiesis is initiated when a multipotent HSPC commits to the erythroid uni-lineage and proceeds through the proliferation and terminal maturation of committed erythroid progenitor cells. Terminal erythropoiesis involves three to five cell divisions,

yielding morphologically distinguishable erythroblasts, including proerythroblasts (Pro-Es), basophilic erythroblasts (Baso-Es), polychromatic erythroblasts (Poly-Es), and orthochromatic erythroblasts (Ortho-Es) [14–17]. Enucleation represents the final stage and is the most distinctive feature of terminal erythroid maturation, which likely constitutes an evolutionary process in mammals. Enucleation is a multistep process resembling asymmetric cytokinesis, commencing with the establishment of cell polarization followed by the formation of a contractile actomyosin ring and the clustering of membrane lipid rafts between reticulocytes and pyrenocyte [18–20].

The optimal outcome of cultured RBCs involves the substantial expansion of stem cells and their precise terminal differentiation into fully mature, functional RBCs, primarily owing to safety concerns. In 2002, Douay group pioneered in vitro RBC generation from CD34+ CB HSPCs, achieving an enucleation rate of 4% [21]. An optimized four-step stroma-free protocol based on Douay group's method was developed by Nakamura group in 2006; this protocol achieved an enucleation rate of approximately 80% from CD34+ CB HSPCs [22]. Attempts to generate RBCs in vitro using hPSCs began in the early 21st century, with various research groups reporting successful differentiation of hPSCs into HSPCs and subsequently into erythroid cells [9, 23, 24]. However, the enucleation rate of erythroids remains low (less than 10%) in hPSCs without stromal cell or macrophage co-culture [25–27].

Before widespread clinical application of hPSC-derived erythrocytes for transfusion and therapy, the molecular mechanisms underlying enucleation defects must be thoroughly investigated. Recent data have indicated that persistent vimentin expression during hPSC-derived erythropoiesis may damage enucleation, although the underlying mechanisms remain unclear [28]. Vimentin is a nuclear anchorage element that extends from the nuclear lamina to the center and periphery of the plasma membrane [29]; it gradually diminishes during differentiation in both murine erythroleukemia cells and murine embryonic erythroid cells [30, 31]. Conversely, in avian erythrocytes, which do not undergo enucleation, vimentin expression is retained and intermediate filaments are strengthened, suggesting a role for vimentin in mammalian erythrocyte enucleation [32, 33]. The knockdown of vimentin by target shRNAs in hPSC-derived erythroid cells results in cell death, leaving the effect of vimentin on enucleation unclear [28].

The proteolysis-targeting chimera (PROTAC) is a potent new technology for inducing target protein degradation via the ubiquitin-proteasome system [34–39]. PROTACs are heterobifunctional molecules that link the ligand of a protein of interest (POI) to an E3 ubiquitin ligase, leading to ubiquitination and subsequent proteasomal degradation of the POI [40–42]. The degradation of target proteins is reversible in a time- and dose-dependent manner, enabling the study of phenotypes that cannot be observed using genetic tools such as CRISPR/Cas9 or RNAi. In one PROTAC method, the degradation tag (dTAG) system utilizes FKBP^{F36V}, a mutated form of FKBP12, as the tag domain that facilitates the degradation of the POI [43–45]. In 2022, the Orkin group first reported in erythropoiesis that globin changes occur upon PROTAC-mediated degradation of the BCL11A protein in erythroid cells [46].

In this study, to verify the importance of vimentin degradation in inducing erythroid differentiation and maturation in stem cells, we utilized the dTAG PROTAC platform to rapidly deplete vimentin protein in erythroid cells and monitored enucleation events during erythropoiesis. We demonstrate that vimentin degradation facilitates enucleation by promoting nuclear polarization during terminal erythroid differentiation. Our findings provide valuable insights into the regulation of erythroid enucleation in hPSC-derived erythroid generation.

Materials and methods

Human subjects
Human CB samples were obtained from the Beijing Umbilical Cord Blood Bank. Women with healthy, full-term pregnancies who met the Beijing Cord Blood Bank criteria for inclusion and provided informed consent were eligible for CB donation. All procedures involving human subjects in this study were approved by the Ethics Committee of the Academy of Military Medical Sciences (AMMS; Approval No. AF/SC-08/02.207).

Induction of hESCs differentiation into erythrocytes and drug treatment
Unless otherwise specified, hESCs were cultured on Matrigel (Corning Life Sciences, Tewksbury, Massachusetts 01876, USA)-coated wells in mTeSR Plus medium (STEMCELL Technology, Vancouver, British Columbia, Canada) according to the manufacturer's protocol. The medium was changed daily and passaged them confluently every 4 to 6 days using ReLeSR (STEMCELL Technology, Vancouver, British Columbia, Canada). Induction of hESCs to form 3D embryoid bodies (EBs), followed by erythroid differentiation requires more than 20 days and involves four distinct phases: (I) mesoderm induction, (II) hemogenic endothelium (HE) commitment, (III) hematopoietic cell emergence and erythroid differentiation, and (IV) erythrocyte maturation (Fig. 1A). Refer to our previous work in our laboratory for detailed culture methods, which were followed with minor modifications [47]. Specifically, 0.5–1 µM of dTAG-7 or dTAG-13 (MCE, Shanghai, China) was added to the medium during the hESC maintenance or erythroblast derivation

stage. The medium containing the drug was replaced with fresh medium when necessary.

Ex vivo hUCB-derived CD34⁺ cell erythroid culture

CD34⁺ hUCB cells were purified using the Human CD34 MicroBead UltraPure Kit (Miltenyi, Gaithersburg, MD, USA). The CD34⁺ cell erythroid differentiation method [48] comprised three phases over 25 days, as follows: (I) HSPC expansion (Day 0–4); (II) erythroid differentiation I (Day 5–15); and (III) erythroid differentiation II (Day 16–25). Cells cultured in expansion medium (StemSpan™ SFEM II, CC100 cytokine cocktail and 2% Penicillin-Streptomycin) at 10^5 cells/mL from day 0 to 4. After expansion, the cells were cultured in Iscove's Modified Dulbecco's medium (IMDM)-based erythroid differentiation medium supplemented with different cytokines in EDM-1 and EDM-2. The medium base for both differentiation phases consists of IMDM, 10% human AB type serum, 5% human AB type plasma, 300 μg/mL holo-human transferrin, 10 μg/mL recombinant human insulin, and 2% Penicillin-Streptomycin. From day 5 to 15, the cells were cultured in EDM-1 medium consisting of erythroid differentiation medium base, 5 ng/mL rhIL-3, 100 ng/mL rhSCF, and 6 IU/mL rhEPO. From day 16 to 25, the cells were grown in EDM-2 medium containing an erythroid differentiation medium base, 50 ng/mL rhSCF, and 6 U/mL rhEPO.

dTAG knock-in vector construction

pVIM expresses the Cas9 protein and single guide RNA (sgRNA). The sgRNA for *vimentin* (*N*-terminal targeted) was designed using the website www.crispr.mit.edu [49]. The donor plasmid of the *vimentin* gene, containing the left and right homology arms, in a *Puromycin-P2A-2×HA-FKBP*^{V} cassette was used for targeting (Additional file S1: Fig. S1). Plasmids were synthesized and purified using VectorBuilder (Yunzhou Biotech, Guangzhou, China).

Generation of the dTAG-VIM-H9 knock-in cell line

For targeting, $1×10^6$ hESCs were electroporated with 2 μg of donor plasmid and 4 μg of *pVIM* plasmid containing two sgRNAs targeting *vimentin* genes. Subsequently, the electroporated hESCs were plated onto matrigel-coated six-well plates supplemented with Y-27,632 (10 μM, Selleck, Shanghai, China) for 1 day. Positive clones were selected by puromycin (2 μg/mL, InVivoGen, San Diego, CA, USA) in mTeSR Plus medium.

PCR detection of knock-in cell clones

To confirm the dTAG-VIM-H9 knock-in clones, genomic DNA was extracted using the TIANamp Genomic DNA kit (TIANGEN, Beijing, China), and PCR was performed using 2 × Phanta Max Master Mix (Dye Plus) (Vazyme, Nanjing, China). The primer set for each gene, including KI-VIM-F1/R1, was used to amplify a 0.7–1.9 Kb product of the targeted integration. A primer set for each gene, including KI-VIM-F2/R2, was used to amplify a 2.3 Kb product to identify whether random integration occurred. The primers used in this study are listed in Table S2 (Additional file 1).

Karyotype analysis

Cells were treated with colchicine (Sigma Aldrich, St. Louis, Missouri, USA) for 3 h, harvested, and then treated with hypotonic solution for karyotype analysis, as previously described [50]. At least 20 metaphase cells for each sample were analyzed with regard to chromosome number and structural rearrangements by the Beijing Capital Bio Medical Laboratory.

Cytospin preparations and benzidine-giemsa staining

First, $5×10^4$ cells were centrifuged onto polylysine-coated slides for 3 min at 500 rpm (CYTOPRO, WESCOR-7622), air-dried, and fixed in −20 °C methanol for 5 min. Benzidine solution was prepared by dissolving one benzidine tablet (Sigma Aldrich, St. Louis, Missouri, USA) in 10 ml of phosphate-buffered saline (PBS) and filtered through a 0.22 μm filter. Ten microliters of 30% hydrogen peroxide solution (Sigma Aldrich, St. Louis, Missouri, USA) was added to the benzidine solution immediately before staining, and then placed as drops directly on the fixed cells for 30 min at room temperature. The cells were briefly rinsed with PBS and stained with Wright–Giemsa solution according to the manufacturer's recommendations (Baso, Zhuhai, China). Solution A was added and allowed to react for 1 min at room temperature, followed by the addition of solution B, and incubation for 8 min. The samples were washed and air dried prior to imaging.

Immunofluorescence staining and imaging (high-content imaging and confocal microscopy)

Cells were cytocentrifuged onto glass slides, fixed with 4% paraformaldehyde for 15 min at room temperature, rinsed with PBS, permeabilized with 0.1% Triton X-100, blocked with 4% bovine serum albumin (BSA) in PBS for 1 h, and then incubated with primary antibodies at 4 ℃ overnight. Isotype-specific secondary antibodies labeled with fluorophores were added when necessary and incubated for 1 h at room temperature. The cells were counterstained with 4′,6-diamidino-2-phenylindole (DAPI) for visualization of cell nuclei and then observed using a high-content imaging system (Perkin Elmer, Waltham, Massachusetts, USA) or a Zeiss LSM 980 confocal microscope (Zeiss, Oberkochen, Germany).

Quantitative real-time PCR

Total RNA from cells was purified using an RNeasy kit (QIAGEN, Valencia, CA, USA). cDNA was prepared from 1 μg of RNA using the ReverTraAce™ qPCR RT Master Mix (TOYOBO, Shanghai, China). PCR was performed using the SYBR qPCR Mix (TOYOBO, Shanghai, China) on a CFX96 Touch Real-Time PCR Detection System (Bio-Rad). Relative gene expression levels were defined according to the comparative Ct method [51] and were normalized to 18 S rRNA expression. The primers used are listed in Table S2 (Additional file S2).

Protein extraction and western blotting

The cells were lysed in RIPA lysis buffer (CWBio, Beijing, China) for total protein extraction. Proper amounts of protein lysates were electrophoresed on 4–20% Fast-PAGE™ Ready Gel (Tsingke, TSP024-12, Beijng, China), transferred to PVDF membranes (0.22 μm) (Merck, Shanghai, China), and probed with anti-HA Tag, anti-VIM, or anti-GAPDH antibodies. Antibody binding was detected using appropriate horseradish peroxidase (HRP)-conjugated IgG and visualized using a GE Amersham Imager (AI680, USA).

Flow cytometric analysis

Flow cytometric analysis was performed using the following antibodies: SSEA4-AF647, TRA1-60, and TRA1-81 for the pluripotency assay of H9 and dTAG-VIM-H9 cell lines. CD309 (KDR)-APC, CD34-BV421, CD31-APC, CD71-APC, and CD235a-FITC were used for H9 and dTAG-VIM-H9 during erythroid differentiation in vitro. Hoechst33342 was used to stain the cell nuclei. The cells were stained at 4 ℃ for 30 min while protected from light. The filtered (40 μm) samples were analyzed on a Guava easyCyte flow cytometer (Luminex, Austin, Texas, USA). All antibodies were purchased from BD Biosciences (Franklin Lakes, NJ, USA) or Invitrogen (Carlsbad, California, USA) (Additional file 1: Table S1). An Annexin V kit (DojinDo Molecular Technologies, Kumamoto, Japan) was used for the apoptosis assay. Data were analysed using Flowjo V10.1 software.

Imaging flow cytometry analysis using imagestream[X] mark II

The distribution of cytoskeletal molecules within the enucleating erythroblasts was analyzed using the Imagestream[X] Mark II platform (Cytek Amnis), which integrates both flow cytometry and microscopy functionalities, employing objective lenses with magnifications of 40× (numerical aperture, 0.75) and 60× (numerical aperture, 0.9). Erythroid cells were harvested in PBS supplemented with 2% fetal bovine serum (FBS) on ice. Next, the cells were centrifuged at 1,000 rpm for 30 s using a benchtop centrifuge and fixed in PBS containing 4% paraformaldehyde for 20 min at room temperature. Formaldehyde was eliminated by centrifugation at 2,000×g for 30 s followed by careful removal of the supernatant, and the resulting cell pellet was cooled on ice for 10 min. Permeabilization was achieved through consecutive immersions in ice-cold acetone solutions of 50%, 100%, and again 50% (maintained at −20 ℃), respectively, with a final wash in fluorescence-activated cell sorting (FACS) buffer [52]. Cells were resuspended in FACS buffer and incubated with CD235a-FITC or CD71-APC. After washing once with FACS buffer, the nuclear stain Hoechst33342 (Thermo Fisher Scientific, Waltham, MA, USA) was added at a concentration of 2 μg/mL in FACS buffer, and the samples were processed using Imagestream[X]. Approximately 20,000 events per experiment were collected and analyzed using the associated Image Data Exploration and Analysis Software (IDEAS). The "Delta Centroid BF-HO" was calculated as the distance of the center of the CD235a-labeled erythroblast from the center of the Hoechst33342-labeled nucleus. A threshold of two for the delta centroid (DC) was established to differentiate between polarized and non-polarized nuclei [53].

Statistical analysis

All experiments were conducted with a minimum of three replicates under similar conditions, and the data are presented as the mean±standard deviation (SD). Statistical significance was determined using a two-tailed *Student's t-test* using GraphPad Prism 10.2 software. A p-value<0.05 was considered statistically significant. Imagestream[X] data, including the centroid distances and bright detail intensities from the experiments depicted in Fig. 5C, were exported for statistical analysis. Both the delta centroid distance and bright detail intensity measurements were non-negative and exhibited an asymmetric probability distribution skewed toward large values, indicating non-normality. Therefore, to assess the statistical significance of the difference in medians between the test and control groups, we used the Wilcoxon rank-sum test, a nonparametric test for two independent samples that makes no assumptions about the underlying probability distributions and is therefore suitable for non-normal data. For each set of measurements, both the mean and median are reported for each group along with the two-tailed p-value obtained from the Wilcoxon rank-sum test.

Results

Vimentin expression dynamics during erythroid differentiation and establishment of the hESC cell line (dTAG-VIM-H9) for vimentin protein degradation

By employing our optimized four-step protocol, human pluripotent stem cells can be induced to differentiate into

erythrocytes in vitro within 30 days [47]. In brief, during the initial and secondary stages of induction culture (first 6 days), pluripotent stem cells completed the formation of 3D embryoid bodies (EBs) and the development of the mesoderm and HE. The early phase of the third stage mainly involves the endothelial-hematopoietic transition, which generates a substantial number of hematopoietic stem progenitor cells, followed by erythroid differentiation initiated by key cytokines such as rhEPO, rhIL-3, and transferrin (Fig. 1A). Initially, we examined the expression profile of vimentin mRNA during erythropoiesis in both hUCB-derived CD34$^+$ cells and the pluripotent stem cell line, H9, in our in vitro culture system. We observed a gradual reduction in vimentin gene expression in CB CD34$^+$ cells by the 10th day of erythroid differentiation, in contrast to sustained high-level expression throughout erythropoiesis in H9 cells (Fig. 1B, C). Additionally, we evaluated vimentin protein levels during erythroid differentiation. Consistent with the transcription level findings, vimentin protein levels progressively declined during erythroid differentiation of CB CD34$^+$ cells (Fig. 1D and Additional file 2: Fig. S6). In contrast, persistence of the VIM protein was observed throughout the erythroid differentiation process in H9 cells (Fig. 1E and Additional file 2: Fig. S6). In accordance with a previous report, the expression of vimentin in CD34$^+$ cells derived from human peripheral blood gradually diminishes during erythroid differentiation, whereas erythroid cells differentiated from hPSCs continue to express vimentin until the orthochromatic erythroblast stage [28]. Vimentin, which functions as an anchor protein in the nucleus of erythroid cells [29], gradually diminishes during the differentiation of murine erythroblasts, coinciding with enucleation [30, 31, 54]. Conversely, avian erythrocytes, which are nucleated, retain vimentin [33], suggesting a role for vimentin in mammalian erythrocyte enucleation.

To ascertain the necessity of vimentin degradation for in vitro-induced erythroid differentiation and maturation, we ectopically expressed VIM fused to a mutated FKBP domain (Fig. 1F), also known as the dTAG system [43, 55]. On the dTAG platform, a dTAGed protein is subjected to degradation by specific chimeric degrader molecules (e.g., dTAG-7, dTAG-13, and dTAG-47), which simultaneously bind to CRBN and FKBP^{F36V} fused to the target protein, inducing molecular proximity and ensuing degradation by the proteasome [43, 46]. The HA-dTAG VIM vector was transfected into the H9 cells via electroporation. Following puromycin selection, several homozygous knock-in clones were confirmed by electrophoresis and sequencing (Fig. 1G, Additional file 1: Fig. S1and Additional file 2: Fig. S7). Both Western blotting and immunofluorescence results confirmed the expression of 2xHA-FKBP^{F36V}-VIM fusion protein ($\sim$70.5 kDa)

in dTAG-VIM-H9 cells (Fig. 1H-I and Additional file 2: Fig. S6).

The dTAG-VIM-H9 cell line exhibited normal characteristics of hPSCs

The dTAG-VIM-H9 cells maintained a normal diploid karyotype (46, XX) and cell morphology (Fig. 2A, B). The pluripotency of dTAG-VIM-H9 cells was confirmed by immunostaining for pluripotency markers (SOX2 and OCT4) (Fig. 2C, D) and flow cytometry analysis of pluripotency markers (SSEA-4, TRA-1-60, and TRA-1-81) (Fig. 2E, F). Subsequently, these cells were effectively induced into erythrocytes within approximately 20 days, which is consistent with the differentiation capability of the conventional pluripotent stem cells, H9 (Fig. 2G–I). In the fourth stage, erythroid cells undergo gradual maturation, which is characterized by a reduction in cell size, nuclear condensation, and polarization, with some erythrocytes successfully undergoing enucleation. This stage was also accompanied by a significant upregulation of hemoglobin (Figs. 2H and I and 5D, and Additional file 1: Fig. S5C, D). Flow cytometry analysis revealed that the expression levels of early mesoderm (KDR), HE (CD31), early hematopoietic markers (CD34 and CD43), early erythroid progenitor marker (CD71), and mature erythroid marker (CD235a) remained consistent between dTAG-VIM-H9 and H9 cells at each stage of erythroid differentiation (Additional file 1: Fig. S3). Upon completion of differentiation, over 96% of the cells in both cell lines expressed the mature erythroid marker CD235a.

dTAG molecules mediated vimentin degradation without affecting cell viability

Based on the investigations conducted by Nabet et al. [43], we selected two prevalent dTAG molecules—dTAG-7 and dTAG-13—to verify whether the HA-dTAG VIM protein of dTAG-VIM-H9 cells could be targeted for degradation. Initially, we added 1 µM dTAG-7 or dTAG-13 to the medium, as previous studies have suggested that 0.5–1 µM dTAG-7/13 molecules can efficiently induce degradation of target proteins across multiple cell lines in a short timeframe [43, 45, 46]. Subsequently, we detected the expression of HA-dTAG VIM protein at the embryonic stem cells culture stage using a high-content imaging system. Immunofluorescence results showed substantial degradation of the HA-dTAG VIM protein (green) within 24 h, regardless of whether dTAG-7 or dTAG-13 was used (Fig. 3A). Statistical analyses conducted using high-content imaging revealed that the average fluorescence intensity of HA-dTAG VIM in the experimental groups supplemented with dTAG-7 or dTAG-13 was significantly lower than that in the control group (None) (Fig. 3B). Additionally, immunofluorescence detection was performed using an anti-HA
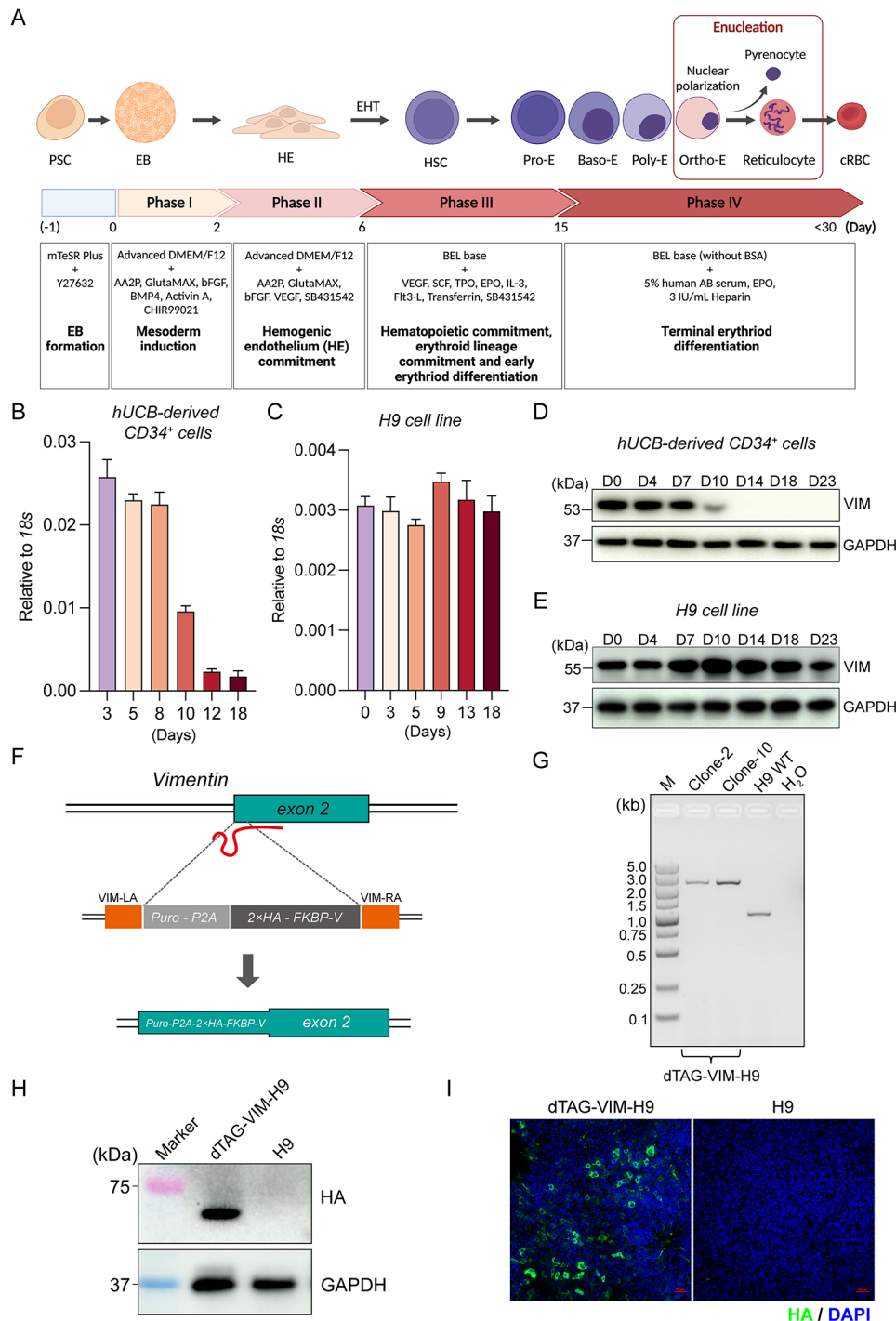
Fig. 1 Vimentin expression dynamics during erythroid differentiation and establishment of the hESC cell line (dTAG-VIM-H9) for vimentin protein degradation. **A** Schematic diagram illustrating the induction of erythroid differentiation from human pluripotent stem cells (hPSCs). PSC, pluripotent stem cell; HSC, hematopoietic stem cell; EB, embryoid body; HE, hemogenic endothelium, Pro-E, proerythroblast; Baso-E, basophilic erythroblast; Poly-E, polychromatic erythroblast; Ortho-E, orthochromatic erythroblast; EHT, endothelial-hematopoietic transition. Created with BioRender.com. **B**, **C** Variation of *VIM* gene expression at different time points during erythroid differentiation between hUCB derived-CD34^{+} cells (**B**) and the H9 cell line (**C**). **D**, **E** Western blot analysis of VIM (54 kDa) in hUCB derived-CD34^{+} cells (**D**) and the H9 cell line (**E**) at different time points during erythroid differentiation (Cropped blots). Source blots are presented in Additional file 2: Fig. S6. **F** Strategy to knock in *FKBP12*[F36V] at the 5' start of *Vimentin*. Puromycin is used as a selection marker. For dTAG knock-in: Vimentin was tagged at the N-terminus with HA-dTAG. **G** Agorose gel analysis of cell clones showed the HA-dTAG fragment was successfully inserted into the target region of the genome of dTAG-VIM-H9 cells (clone-2 and clone-10) (Cropped gel). Uncropped gel is presented in Additional file 2: Fig. S7. **H** Verification of dTAG-VIM (∼70.5 kDa) expression by Western blot analysis (Cropped blots). Source blots are presented in Additional file 2: Fig. S6. **I** Immunofluorescence (HA-Tag) detection of HA-dTAG VIM protein in dTAG-VIM-H9 cells. Scale bar = 50 μm
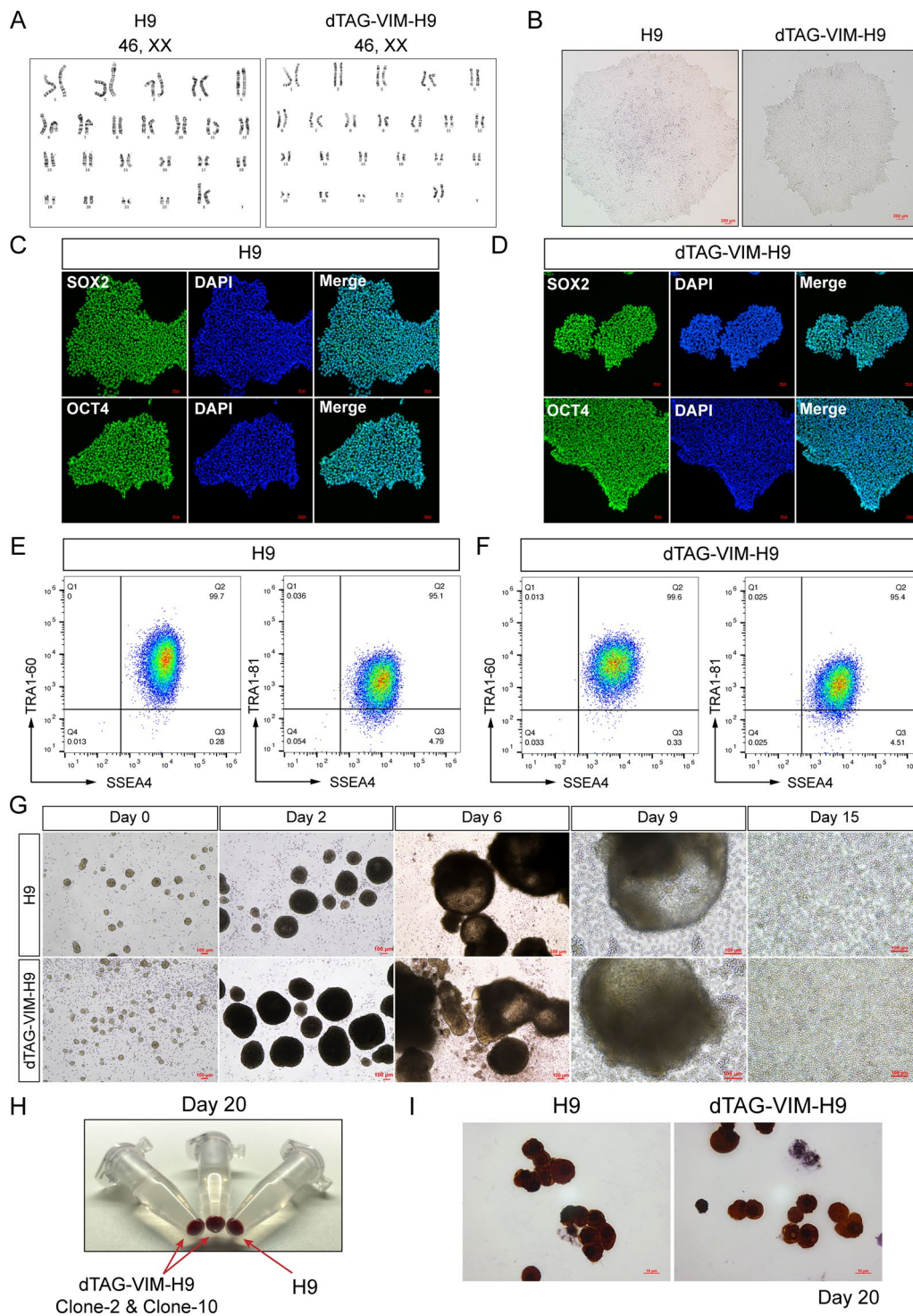
Fig. 2 The dTAG-VIM-H9 cell line exhibited normal characteristics of hPSCs. **A** A representative normal karyotype of H9 and dTAG-VIM-H9 cells. **B** H9 and dTAG-VIM-H9 cells exhibit normal morphology. Scale bar = 100 μm. **C**, **D** Immunofluorescence staining showing presence of pluripotency markers SOX2 and OCT4 in H9 (**C**) and dTAG-VIM-H9 (**D**) cells. Scale bar = 20 μm. **E**, **F** H9 (**E**) and dTAG-VIM-H9 (**F**) cells express hESC surface markers (SSEA4, TRA-1-60, TRA-1-81). **G** H9 and dTAG-VIM-H9 cells exhibited consistent morphological changes throughout the 18-day in vitro erythroid differentiation process, ultimately successfully differentiating into erythroid cells. Scale bar = 100 μm. **H** Corresponding cRBC pellets from the different hPSC lines on day 20 (erythroid differentiation-day 14) of induction. **I** Benzidine-Giemsa staining of H9- or dTAG-VIM-H9-derived erythrocytes on day 20. Scale bar = 10 μm
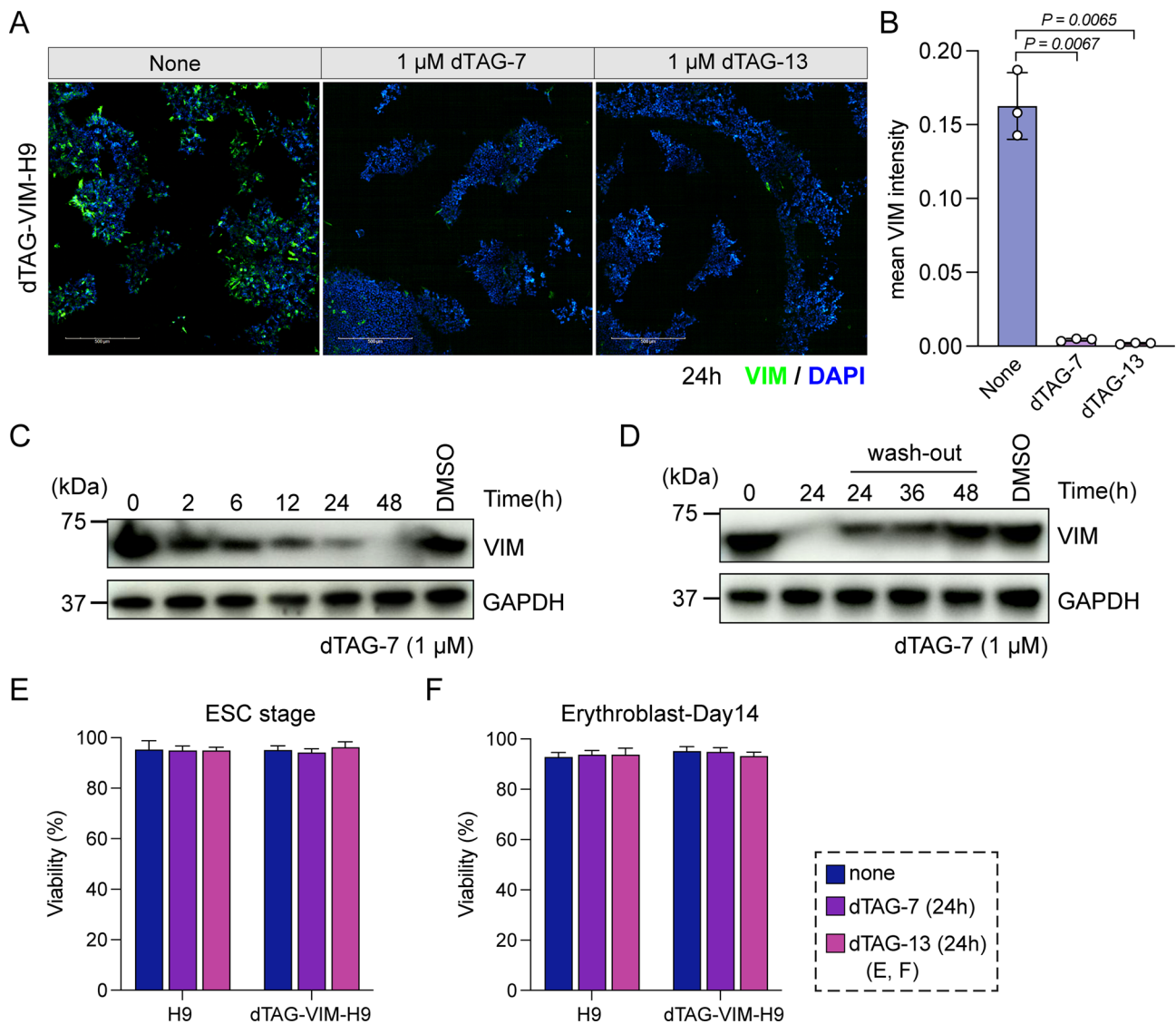
Yan *et al. Stem Cell Research & Therapy*   (2024) 15:310

Page 9 of 15

Fig. 3 dTAG molecules mediated vimentin degradation without affecting cell viability. **A** Expression, re-localization, and degradation of HA-dTAG Vimentin were monitored by immunofluorescence and quantified by automated image analysis. Scale bar = 500 μm. **B** High-content imaging data revealed a statistically significant decrease in the mean fluorescence intensity of VIM proteins after 24 h of treatment with 1 μM dTAG-7/13. **C** Western blot of dTAG-VIM (∼ 70.5 kDa) in dTAG-VIM-H9 cells treated with 1 μM dTAG-7 (Cropped blots). Source blots are presented in Additional file 2: Fig. S8. **D** Western blot of dTAG-VIM (∼ 70.5 kDa) upon DMSO or dTAG-7 treatment for 24 h, followed by wash-out of dTAG-7 at various times in dTAG-VIM-H9 cells (Cropped blots). Source blots are presented in Additional file 2: Fig. S8. **E**, **F** Viability analysis of H9 and dTAG-VIM-H9 cells after 24 h of treatment with 1 μM dTAG-7/13 at the ESC maintainance stage (**E**) and erythroblast stage (**F**)

antibody, demonstrating the degradation of HA-dTAG VIM protein within 24 h under the influence of 1 μM dTAG-7 (Additional file 1: Fig. S2).

To assess the reversibility of the protein degradation induced by PROTACs (dTAG-7), we conducted a wash-out experiment with dTAG-7. Subsequent to incubating dTAG-VIM-H9 cells with 1 μM dTAG-7 for 24 h, dTAG-7 was washed-out and replaced with a fresh medium to observe the alterations in VIM protein expression. Following the washout experiment, VIM exhibited rapid and complete recovery within 48 h (Fig. 3C, D and Additional file 2: Fig. S8). Furthermore, we confirmed that 1 μM

dTAG-7/13 molecules had no significant impact on cell viability at either the embryonic stem cells maintanance stage or erythroblast induction stage, as cell viability remained approximately 95% (Fig. 3E, F).

Vimentin degradation moderately enhances the enucleation in dTAG-VIM-H9 cells during erythroid differentiation

To verify whether VIM protein could also undergo degradation mediated by dTAG molecules during erythroid differentiation, we supplemented the culture system with 0.5 μM dTAG-7 on the 13th day of culture (7th day

of erythroid differentiation, ED-day 7). Three days later, the immunofluorescence results demonstrated significant degradation of the HA-dTAG VIM protein (red) (Fig. 4A and Additional file 1: Fig. S4A). The VIM protein in dTAG-VIM-H9 cells at the erythroid differentiation stage was completely degraded within 12 h (Fig. 4B and Additional file 2: Fig. S9), and the cells did not undergo apoptosis owing to the action of dTAG-7 (Fig. 4C, D). Importantly, erythroid differentiation was unaffected in

the dTAG-7 treated group. The expression of erythroid surface markers (CD71, CD235a) on the 20th day (ED-day 14) was essentially consistent between the dTAG-7 treated group (dTAG-VIM-H9 cells), untreated (dTAG-VIM-H9 cells), and WT (H9 cells) groups (Additional file 1: Fig. S4B). Notably, the proportion of CD235$^+$CD71$^-$ cells in the dTAG-7-treated dTAG-VIM-H9 was significantly higher compared to the untreated group (Fig. 4E). We further assessed the the proportion of enucleated
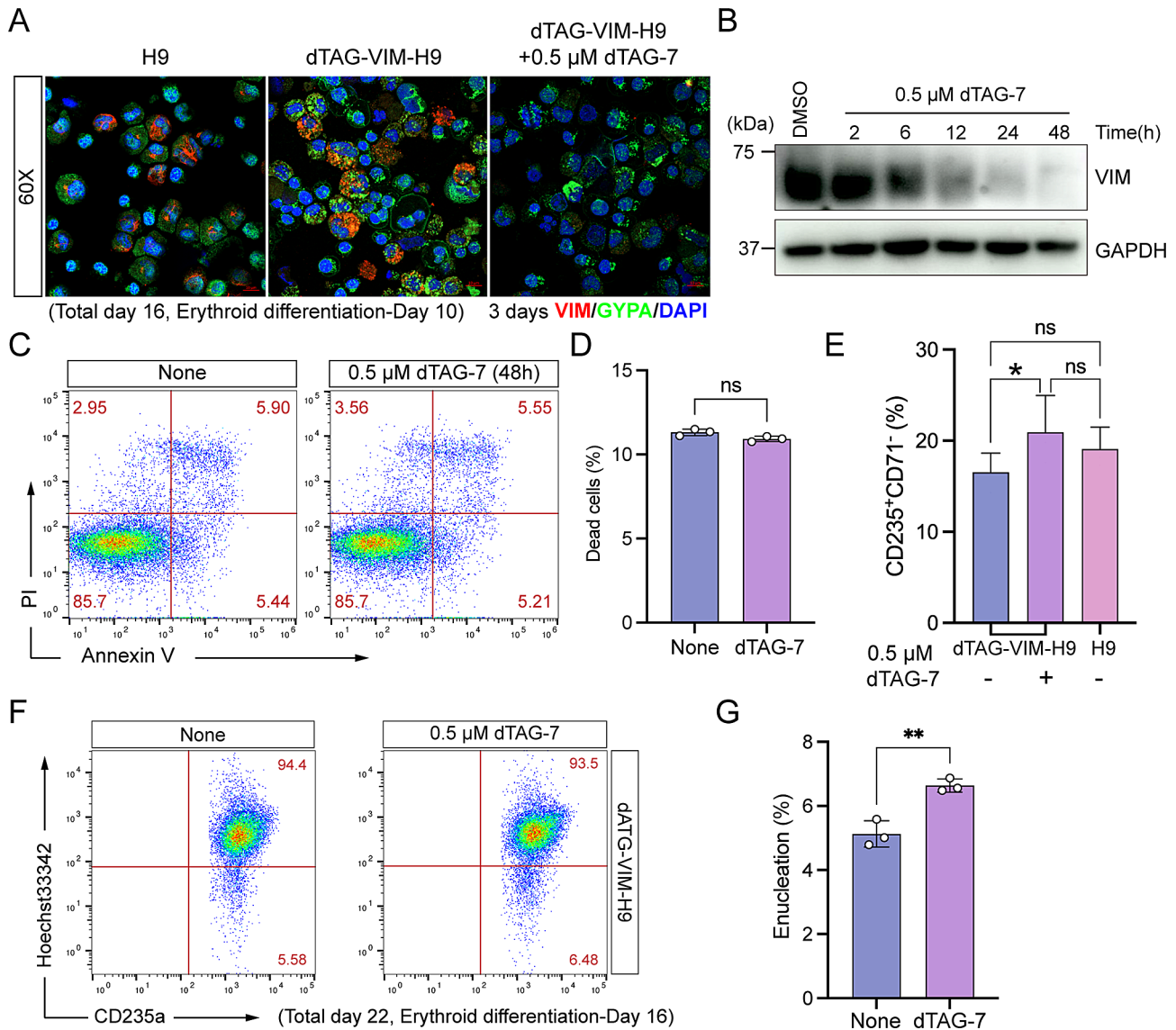

Fig. 4 Vimentin degradation moderately enhances the enucleation rate in dTAG-VIM-H9 cells during erythroid differentiation. **A** Immunofluorescence staining of VIM, GYPA, and DAPI was conducted in cultured H9 or dTAG-VIM-H9 erythroblasts on the 14th day. Scale bars = 10 μm (60X). **B** Western blot analysis of dTAG-VIM protein (∼70.5 kDa) at various time points (2 h, 6 h, 12 h, 24 h and 48 h) following treatment with 0.5 μM dTAG-7 (Cropped blots). Source blots are presented in Additional file 2: Fig. S9. **C** Flow cytometric analysis of apoptosis of dTAG-VIM-H9 cells induced for 14 days of erythroid differentiation following 48 h of treatment with 0.5 μM dTAG-7, using annexin V and propidium iodide (PI). **D** Quantitative analysis of (**C**). Data was obtained from three independent experiments. **E** Quantitative analysis of CD235$^+$CD71$^-$ cells on the 14th day of erythroid culture by flow cytometry. Data were obtained from three independent experiments (Related to Fig. S4B). **F** Flow cytometric analysis of erythroid markers and nuclear dye (CD235a, Hoechst33342) on 16th day of dTAG-VIM-H9 erythroid culture. The CD235a$^+$Hoechst$^-$ population represents enucleated erythrocytes. **G** Statistical analysis of enucleated erythrocytes following treatment with 0.5 μM dTAG-7. Data was obtained from three independent experiments (Related to F)

erythrocytes (CD235a$^+$Hoechst33342$^-$) at the late stage of erythroid differentiation (ED-day16, total day 22) using flow cytometry. It's indicated that under culture conditions with 0.5 μM dTAG-7, dTAG-VIM-H9 cells showed an increased proportion of enucleated erythrocytes (approximately 6.5%) (Fig. 4F, G). In contrast, the proportions of enucleated erythrocytes are significant lower in the untreated group and WT group (Additional file 1: Fig. S5A, B).

Additionally, during the erythroid induction phase, we examined the expression of the *vimentin* in dTAG-VIM-H9 and H9 cells. At ED-day 3, the relative expression of *vimentin* in dTAG-VIM-H9 cells was significantly lower than that in H9 cells (WT group) (Additional file 1: Fig. S4C). At the subsequent three time points (ED-day 6, 14, and 20), the expression of vimentin in erythroid cells derived from dTAG-VIM-H9 did not exhibit a consistent change with the dTAG-7-mediated degradation of VIM protein (Additional file 1: Fig. S4D–F), suggesting that PROTAC-mediated protein degradation did not have a notable impact on the transcriptional process of the target gene.

Targeted vimentin degradation promotes nuclear polarization in preparation for enucleation during erythroid differentiation

Terminal maturation of erythropoiesis involves nuclear condensation, nuclear polarization, and enucleation [56] (Fig. 1A). To demonstrate that targeted degradation of the cytoskeletal protein VIM promotes nuclear polarization, we used imaging flow cytometry to measure the distance between the nuclear and cellular centers, using these data to assess the degree of nuclear polarization (a greater distance indicates higher polarization) (Fig. 5A, B). Statistical analysis of the Imagestream^X data, measuring the parameter delta-centroid BF-HO (which represents the distance between the center of the cell body observed in the bright field and the center of the nuclear staining achieved with Hoechst33342, HO) demonstrated that dTAG-7-mediated targeted degradation of VIM promoted nuclear polarization in maturing erythrocytes (Fig. 5C).

Moreover, following cytospin preparation, staining with Benzidine–Giemsa revealed erythroid cells in a reddish-brown hue, while non-erythroid cells appeared pale purple (Fig. 5D). The cells were classified based on whether the nucleus was localized at the center of the cells (centered) or whether the cells were spherical and contained a condensed nucleus located on one side close to the plasma membrane (polarized). Other cell types, such as multinucleate and non-erythroid cells, including macrophages, were classified as "others" [57]. Statistical analysis of the proportions of the three cell types revealed a significantly higher percentage of cells exhibiting

nuclear polarization in the dTAG-VIM-H9 cells cultured with dTAG-7 than in the untreated and WT groups (H9 cells) (Fig. 5E). By day 20 of erythroid culture (total day 26), a higher proportion of CD235$^+$CD71$^-$ erythrocytes was observed in the dTAG-7 treated group compared to the untreated group (45.8% vs. 29.4%). Additionally, Benzidine–Giemsa staining showed an increased number of erythroid cells displaying nuclear polarization (indicated by red arrows) and enucleated RBCs (Additional file 1: Fig. S5C, D).

Discussion

To explore the potential involvement of vimentin in regulating enucleation during erythropoiesis, we initially utilized the target protein degradation platform PROTAC to establish an inducible hESC line named dTAG-VIM-H9. dTAG induced the degradation of vimentin within 12 h. In contrast to the lethal effect observed following vimentin mRNA knockdown by shRNAs [28], vimentin protein degradation had no significant impact on cell viability. Subsequently, dTAG-VIM-H9 cells differentiated into erythroid cells with or without the addition of the dTAG molecule. Vimentin degradation occurs in the presence of dTAG, resulting in enhanced enucleation, indicating that vimentin negatively regulates erythrocyte enucleation without altering apoptosis. Furthermore, more erythroid cells exhibited nuclei located farther from the central location upon vimentin degradation, suggesting that vimentin fine-tuning mediates erythroblast nuclear polarization in preparation for enucleation.

Previous studies have demonstrated that cytoskeletal systems composed of intermediate filaments (IFs), actin filaments, microtubules, and myosin interact with each other and exhibit interconnected functions in cell cytokinesis, morphogenesis, and mechano-responsiveness [58]. Enucleation is a multistep process that resembles cytokinesis, initiated by the establishment of cell nucleus polarization through microtubule function, followed by the contraction of asymmetrically localized cytoplasmic actin stress fibers and actomyosin, and the coalescence of lipid rafts between reticulocytes and pyrenocytes [59]. Microtubules mediate erythroblast polarization during preparation for enucleation. Inhibition of tubulin polymerization or depolymerization impedes enucleation by inhibiting erythroblast polarization [55]. Actin is well known to play a critical role in terminal erythropoiesis, particularly enucleation. Blocking actin polymerization completely inhibits erythroblast enucleation [60]. Rac and Rho GTPases are actin remodeling proteins involved in the enucleation regulatory system [15, 61, 62]. It has been demonstrated that Rac/Rho GTPases regulate enucleation through mDia2 activation, which mediates the formation of the contractile actin ring (CAR) between the pycnotic nucleus and incipient reticulocyte [63, 64].
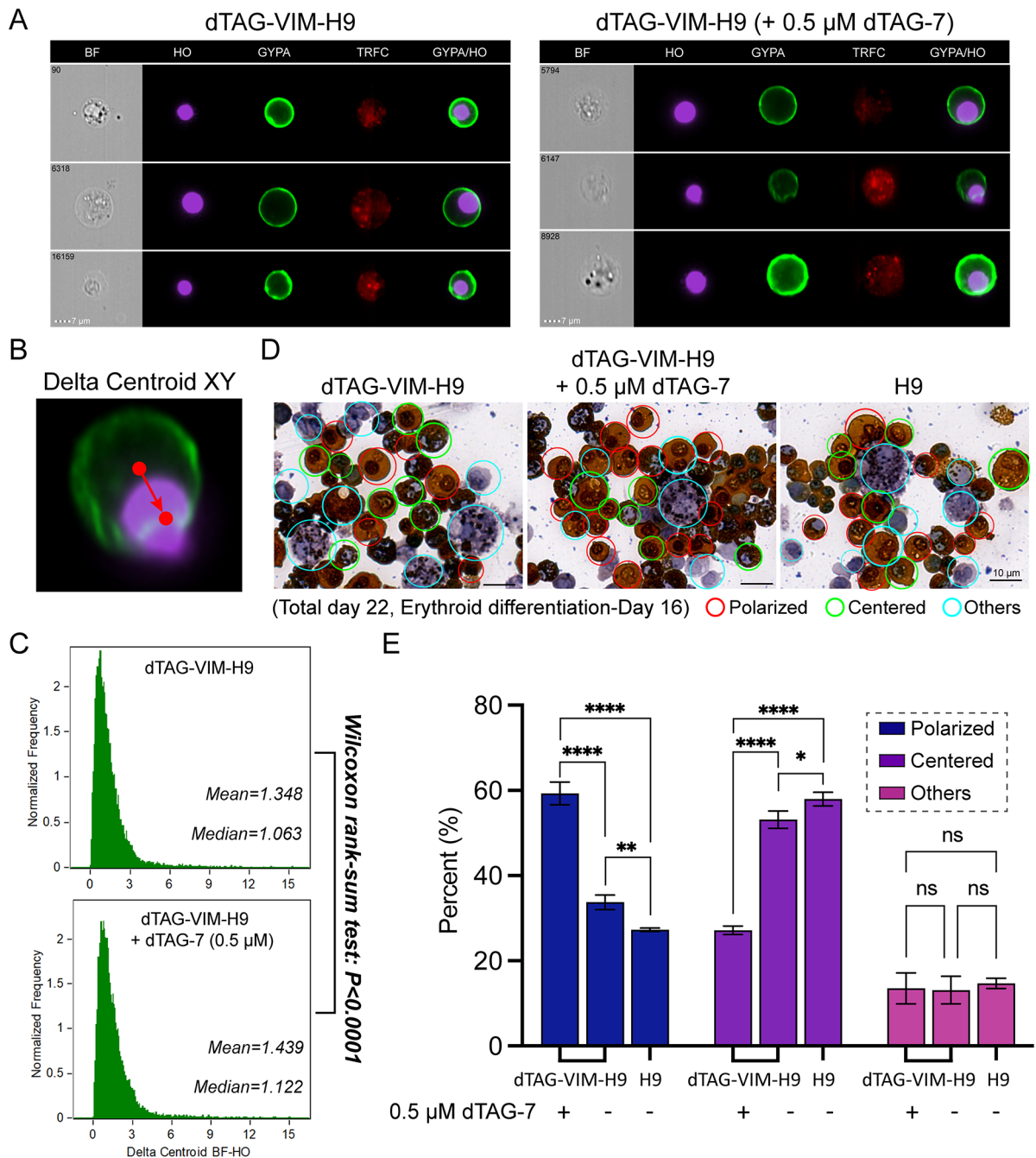
Fig. 5 Targeted vimentin degradation promotes nuclear polarization in preparation for enucleation during erythroid differentiation. **A** Representative images of dTAG-VIM-H9 cells cultured for 16 days in erythroid differentiation, stained with CD71-APC, CD235a-FITC (GYPA) and Hoechst33342 (HO). Left: no treated, Right: 0.5 μM dTAG-7 treated. Scale bar = 7 μm. **B** Representative image of nuclear polarization, where the Delta Centroid XY parameter represents the distance between the cell body center and the nucleus center. **C** The degradation of VIM protein mediated by dTAG-7 resulted in the enhancement of nuclear polarization, as evidenced by the distribution of the parameter Delta Centroid BF-HO. This parameter measures the distance between the center of the cell body observed in bright-field microscopy and the center of the nuclear staining achieved with Hoechst33342 (HO). The median and mean values of the Delta Centroid BF-HO of control and dTAG7-treated dTAG-VIM-H9 erythroblasts are presented, and the difference between the two samples is statistically significant ($P < 0.0001$). **D** Representative images of typical cells classified as polarized (cell containing a condensed nucleus located to one side, close to the plasma membrane. Red circle), centered (nucleus localized at the center of the cells. Green circle), and others (multinucleate or non-erythroid cells. Sky blue circle). Cells are stained with Benzidine and Giemsa reagent. Scale bar = 10 μm. **E** Statistical analysis of the proportion of dTAG-VIM-H9-derived erythroid cells undergoing nuclear polarization under culture conditions with or without 0.5 μM dTAG-7. Erythroid cells derived from H9 served as a WT control. Data were obtained from three independent replicate experiments (Related to D)

As a type III intermediate filament, vimentin forms a vast intracellular network surrounding the nucleus and extends to the cell periphery to anchor organelles, thereby contributing to cellular rigidity and shape [65]. One study shed light on the interplay between vimentin intermediate filament and other cytoskeletal components in terminal erythropoiesis. In 2017, Jiu et al. reported that upon vimentin depletion, actin stress fiber assembly and contractility increased; they confirmed that vimentin affected the assembly and contractility of actin stress fibers by downregulating GEF-H1 and RhoA. Vimentin inactivates GEF-H1 by modulating its phosphorylation at Ser886 [66]. GEF-H1, a nucleotide exchange factor, mediates the crosstalk between microtubules and Rho-dependent regulation of the actin cytoskeleton [67]. RhoA, a member of the Rho GTPase family of proteins, is a major regulator of actomyosin contractility and vesicular trafficking, and plays a significant role in cytokinesis [68–70]. RhoA also regulates myosin regulatory light-chain phosphorylation and microtubule organization during erythroblast cytokinesis, participating in the formation of a transient midbody before abscission [71]. Moreover, VopO has been shown to bind GEF-H1 and, consequently, activate the RhoA-ROCK pathway and actin stress fiber formation [72].

Mechanistically, based on previous studies and our study, we speculate that the retained vimentin IFs in hPSC-induced erythropoiesis may affect terminal maturation through their negative roles in nuclear polarization and actin and actomyosin contractility. Specifically, upon vimentin degradation, GEF-H1, Rac, and RhoA GTPases are activated, promoting nuclear polarization, actomyosin and actin stress fiber assembly, and contractility, thus accelerating terminal maturation.

Notwithstanding that vimentin protein degradation moderately enhances nuclear polarization and enucleation in H9-induced erythropoiesis, enucleation remains insufficient due to its inherent complexity and the limitation of the dish-culture system. Further investigation is required to elucidate the regulatory pathways of vimentin in erythropoiesis. The optimal timing of vimentin degradation for enhancing enucleation also remains to be investigated.

Conclusion

Our study elucidates the critical role of vimentin in regulating erythroid enucleation in hPSCs. Utilizing the dTAG PROTAC platform, we established an inducible hESC line, dTAG-VIM-H9, enabling the rapid and revgrersible degradation of vimentin. Our findings demonstrate that vimentin depletion enhances nuclear polarization and terminal maturation, providing valuable insights into the regulation of erythroid enucleation in hPSC-derived erythroid generation (Graphic Abstract). It is unsurprising that our study provides a proof of concept for the potential therapeutic application of vimentin-targeted PROTACs. Our work also offers a feasible framework for functional studies of targets in erythropoiesis.

Abbreviations

Baso-E	Basophilic Erythroblast
BM	Bone Marrow
CB	Cord Blood
DAPI	4′,6-Diamidino-2-Phenylindole
dTAG	Degradation Tag
EB	Embryoid Body
ED	Erythroid Differentiation
HE	Hemogenic Endothelium
hiPSC	Human Induced Pluripotent Stem Cell
hPSC	Human Pluripotent Stem Cell
hESC	Human Embryonic Stem Cell
HO	Hoechst33342
HSCs	Hematopoietic Stem Cells
HSPCs	Hematopoietic Stem and Progenitor Cells
hUCB	Human Umbilical Cord Blood
IFs	Intermediate Filaments
PI	Propidium Iodide
Ortho-E	Orthochromatic Erythroblast
POI	Protein of Interest
Poly-E	Polychromatic Erythroblast
PROTAC	Proteolysis-Targeting Chimera
Pro-E	Proerythroblast
RBCs	Red Blood Cells
VIM	Vimentin

Supplementary Information

The online version contains supplementary material available at https://doi.org/10.1186/s13287-024-03910-1.

Supplementary Material 1

Supplementary Material 2

Data availability
All data set are available from the corresponding author upon reasonable request.

Declarations

Ethical approval
Human cord blood samples were obtained from Beijing Umbilical Cord Blood Bank. Women with healthy, full-term pregnancies who met the Beijing Cord Blood Bank criteria for inclusion and gave informed consent for participation in the study were eligible to donate cord blood. All procedures involving human subjects in this study were approved by Ethics Committee of Academy of Military Medical Sciences (AMMS) ((1) Title of the approved project: Single-cell Lineage Tracing to Explore the Erythroid Differentiation in Pluripotent Stem Cell. (2) Name of the committee: Committee of Academy of Military Medical Sciences (AMMS). (3) Approval No.: AF/SC-08/02.178. (4) Date of approval: March 11th, 2022).

Consent for publication
All authors confirm their consent for publication.

Competing interests
The authors declare that they have no competing interests.

Author details
[1]Beijing Institute of Radiation Medicine, Beijing 100850, P. R. China

References
1. Cervellera CF, Mazziotta C, Di Mauro G, Iaquinta MR, Mazzoni E, Torreggiani E, Tognon M, Martini F, Rotondo JC. Immortalized erythroid cells as a novel frontier for in vitro blood production: current approaches and potential clinical application. Stem Cell Res Ther. 2023;14(1):139.
2. Red Cross declares emergency blood shortage, calls for donations during National Blood Donor Month. [https://www.redcross.org/about-us/news-and-events/press-release/2024/red-cross-declares-emergency-blood-shortage-calls-for-donations-during-national-blood-donor-month.html]]
3. Fibach E, Manor D, Oppenheim A, Rachmilewitz EA. Proliferation and maturation of human erythroid progenitors in liquid culture. Blood. 1989;73(1):100–3.
4. Wada H, Suda T, Miura Y, Kajii E, Ikemoto S, Yawata Y. Expression of major blood group antigens on human erythroid cells in a two phase liquid culture system. Blood. 1990;75(2):505–11.
5. Fibach E, Rachmilewitz EA. A two-step liquid culture–a novel culture procedure for studying erythroid cell development. Haematologia (Budap). 1991;24(4):211–20.
6. Giarratana MC, Kobari L, Lapillonne H, Chalmers D, Kiger L, Cynober T, Marden MC, Wajcman H, Douay L. Ex vivo generation of fully mature human red blood cells from hematopoietic stem cells. Nat Biotechnol. 2005;23(1):69–74.
7. Takahashi K, Yamanaka S. Induction of pluripotent stem cells from mouse embryonic and adult fibroblast cultures by defined factors. Cell. 2006;126(4):663–76.
8. Thomson JA, Itskovitz-Eldor J, Shapiro SS, Waknitz MA, Swiergiel JJ, Marshall VS, Jones JM. Embryonic stem cell lines derived from human blastocysts. Science. 1998;282(5391):1145–7.
9. Kaufman DS, Hanson ET, Lewis RL, Auerbach R, Thomson JA. Hematopoietic colony-forming cells derived from human embryonic stem cells. Proc Natl Acad Sci U S A. 2001;98(19):10716–21.
10. Vodyanik MA, Bork JA, Thomson JA, Slukvin II. Human embryonic stem cell-derived CD34 + cells: efficient production in the coculture with OP9 stromal cells and analysis of lymphohematopoietic potential. Blood. 2005;105(2):617–26.
11. Klimchenko O, Mori M, Distefano A, Langlois T, Larbret F, Lecluse Y, Feraud O, Vainchenker W, Norol F, Debili N. A common bipotent progenitor generates the erythroid and megakaryocyte lineages in embryonic stem cell-derived primitive hematopoiesis. Blood. 2009;114(8):1506–17.
12. Lee SJ, Jung C, Oh JE, Kim S, Lee S, Lee JY, Yoon YS. Generation of Red Blood cells from human pluripotent stem Cells-An update. Cells 2023, 12(11).
13. Orkin SH. Diversification of haematopoietic stem cells to specific lineages. Nat Rev Genet. 2000;1(1):57–64.
14. Gregory CJ, Eaves AC. Human marrow cells capable of erythropoietic differentiation in vitro: definition of three erythroid colony responses. Blood. 1977;49(6):855–64.
15. Ji P, Jayapal SR, Lodish HF. Enucleation of cultured mouse fetal erythroblasts requires rac GTPases and mDia2. Nat Cell Biol. 2008;10(3):314–21.
16. Hattangadi SM, Wong P, Zhang L, Flygare J, Lodish HF. From stem cell to red cell: regulation of erythropoiesis at multiple levels by multiple proteins, RNAs, and chromatin modifications. Blood. 2011;118(24):6258–68.
17. Keerthivasan G, Liu H, Gump JM, Dowdy SF, Wickrema A, Crispino JD. A novel role for survivin in erythroblast enucleation. Haematologica. 2012;97(10):1471–9.
18. Gifford SC, Derganc J, Shevkoplyas SS, Yoshida T, Bitensky MW. A detailed study of time-dependent changes in human red blood cells: from reticulocyte maturation to erythrocyte senescence. Br J Haematol. 2006;135(3):395–404.
19. Migliaccio AR. Erythroblast enucleation. Haematologica. 2010;95(12):1985–8.
20. Caulier AL, Sankaran VG. Molecular and cellular mechanisms that regulate human erythropoiesis. Blood. 2022;139(16):2450–9.
21. Neildez-Nguyen TM, Wajcman H, Marden MC, Bensidhoum M, Moncollin V, Giarratana MC, Kobari L, Thierry D, Douay L. Human erythroid cells produced ex vivo at large scale differentiate into red blood cells in vivo. Nat Biotechnol. 2002;20(5):467–72.
22. Miharada K, Hiroyama T, Sudo K, Nagasawa T, Nakamura Y. Efficient enucleation of erythroblasts differentiated in vitro from hematopoietic stem and progenitor cells. Nat Biotechnol. 2006;24(10):1255–6.
23. Ma F, Ebihara Y, Umeda K, Sakai H, Hanada S, Zhang H, Zaike Y, Tsuchida E, Nakahata T, Nakauchi H, et al. Generation of functional erythrocytes from human embryonic stem cell-derived definitive hematopoiesis. Proc Natl Acad Sci U S A. 2008;105(35):13087–92.
24. Olivier EN, Qiu C, Velho M, Hirsch RE, Bouhassira EE. Large-scale production of embryonic red blood cells from human embryonic stem cells. Exp Hematol. 2006;34(12):1635–42.
25. Cho YK, Kim HK, Kwon SS, Jeon SH, Cheong JW, Nam KT, Kim HS, Kim S, Kim HO. In vitro erythrocyte production using human-induced pluripotent stem cells: determining the best hematopoietic stem cell sources. Stem Cell Res Ther. 2023;14(1):106.
26. Han H, Rim YA, Ju JH. Recent updates of stem cell-based erythropoiesis. Hum Cell. 2023;36(3):894–907.
27. Pavani G, Klein JG, Nations CC, Sussman JH, Tan K, An HH, Abdulmalik O, Thom CS, Gearhart PA, Willett CM, et al. Modeling primitive and definitive erythropoiesis with induced pluripotent stem cells. Blood Adv. 2024;8(6):1449–63.
28. Trakarnsanga K, Ferguson D, Daniels DE, Griffiths RE, Wilson MC, Mordue KE, Gartner A, Andrienko TN, Calvert A, Condie A, et al. Vimentin expression is retained in erythroid cells differentiated from human iPSC and ESC and indicates dysregulation in these cells early in differentiation. Stem Cell Res Ther. 2019;10(1):130.
29. Xue SP, Zhang SF, Du Q, Sun H, Xin J, Liu SQ, Ma J. The role of cytoskeletal elements in the two-phase denucleation process of mammalian erythroblasts in vitro observed by laser confocal scanning microscope. Cell Mol Biol (Noisy-le-grand). 1997;43(6):851–60.
30. Ngai J, Capetanaki YG, Lazarides E. Differentiation of murine erythroleukemia cells results in the rapid repression of vimentin gene expression. J Cell Biol. 1984;99(1 Pt 1):306–14.
31. Sangiorgi F, Woods CM, Lazarides E. Vimentin downregulation is an inherent feature of murine erythropoiesis and occurs independently of lineage. Development. 1990;110(1):85–96.
32. Granger BL, Repasky EA, Lazarides E. Synemin and vimentin are components of intermediate filaments in avian erythrocytes. J Cell Biol. 1982;92(2):299–312.
33. Granger BL, Lazarides E. Structural associations of synemin and vimentin filaments in avian erythrocytes revealed by immunoelectron microscopy. Cell. 1982;30(1):263–75.
34. Sakamoto KM, Kim KB, Kumagai A, Mercurio F, Crews CM, Deshaies RJ. Protacs: chimeric molecules that target proteins to the Skp1-Cullin-F box complex for ubiquitination and degradation. Proc Natl Acad Sci U S A. 2001;98(15):8554–9.
35. Toure M, Crews CM. Small-molecule PROTACS: New approaches to protein degradation. Angew Chem Int Ed Engl. 2016;55(6):1966–73.
36. Walczak MJ, Petzold G, Thoma NH. Targeted protein degradation: you can glue it too! Nat Chem Biol. 2017;13(5):452–3.
37. Neklesa TK, Winkler JD, Crews CM. Targeted protein degradation by PROTACs. Pharmacol Ther. 2017;174:138–44.

38. Sun X, Gao H, Yang Y, He M, Wu Y, Song Y, Tong Y, Rao Y. PROTACs: great opportunities for academia and industry. Signal Transduct Target Ther. 2019;4:64.

39. Xie X, Yu T, Li X, Zhang N, Foster LJ, Peng C, Huang W, He G. Recent advances in targeting the undruggable proteins: from drug discovery to clinical trials. Signal Transduct Target Ther. 2023;8(1):335.

40. Gadd MS, Testa A, Lucas X, Chan KH, Chen W, Lamont DJ, Zengerle M, Ciulli A. Structural basis of PROTAC cooperative recognition for selective protein degradation. Nat Chem Biol. 2017;13(5):514–21.

41. Nowak RP, DeAngelo SL, Buckley D, He Z, Donovan KA, An J, Safaee N, Jedrychowski MP, Ponthier CM, Ishoey M, et al. Plasticity in binding confers selectivity in ligand-induced protein degradation. Nat Chem Biol. 2018;14(7):706–14.

42. An S, Fu L. Small-molecule PROTACs: an emerging and promising approach for the development of targeted therapy drugs. EBioMedicine. 2018;36:553–62.

43. Nabet B, Roberts JM, Buckley DL, Paulk J, Dastjerdi S, Yang A, Leggett AL, Erb MA, Lawlor MA, Souza A, et al. The dTAG system for immediate and target-specific protein degradation. Nat Chem Biol. 2018;14(5):431–41.

44. Simpson LM, Glennie L, Brewer A, Zhao JF, Crooks J, Shpiro N, Sapkota GP. Target protein localization and its impact on PROTAC-mediated degradation. Cell Chem Biol. 2022;29(10):1482–e15041487.

45. Bensimon A, Pizzagalli MD, Kartnig F, Dvorak V, Essletzbichler P, Winter GE, Superti-Furga G. Targeted degradation of SLC transporters reveals amenability of Multi-pass transmembrane proteins to Ligand-Induced Proteolysis. Cell Chem Biol. 2020;27(6):728–e739729.

46. Mehta S, Buyanbat A, Kai Y, Karayel O, Goldman SR, Seruggia D, Zhang K, Fujiwara Y, Donovan KA, Zhu Q, et al. Temporal resolution of gene derepression and proteome changes upon PROTAC-mediated degradation of BCL11A protein in erythroid cells. Cell Chem Biol. 2022;29(8):1273–e12871278.

47. Xu L, Zeng Q, Liang L, Yang Z, Qu M, Li H, Zhang B, Zhang J, Yuan X, Chen L, et al. Generation of Rh D-negative blood using CRISPR/Cas9. Cell Prolif. 2023;56(11):e13486.

48. Li D, Wu F, Zhou S, Huang XJ, Lee HY. Heterochromatin rewiring and domain disruption-mediated chromatin compaction during erythropoiesis. Nat Struct Mol Biol. 2023;30(4):463–74.

49. Hsu PD, Scott DA, Weinstein JA, Ran FA, Konermann S, Agarwala V, Li Y, Fine EJ, Wu X, Shalem O, et al. DNA targeting specificity of RNA-guided Cas9 nucleases. Nat Biotechnol. 2013;31(9):827–32.

50. Li H, Pei H, Nie J, Qu M, Fan Z, Jia Y, He L, Nan X, Yue W, Pei X. Integration-free reprogramming of human umbilical arterial endothelial cells into induced pluripotent stem cells IHSTMi001-A. Stem Cell Res. 2018;31:231–4.

51. Livak KJ, Schmittgen TD. Analysis of relative gene expression data using real-time quantitative PCR and the 2(-Delta Delta C(T)) method. Methods. 2001;25(4):402–8.

52. Thorpe SJ, Thein SL, Sampietro M, Craig JE, Mahon B, Huehns ER. Immunochemical estimation of haemoglobin types in red blood cells by FACS analysis. Br J Haematol. 1994;87(1):125–32.

53. Moras M, Hattab C, Gonzalez-Menendez P, Fader CM, Dussiot M, Larghero J, Le Van Kim C, Kinet S, Taylor N, Lefevre SD, et al. Human erythroid differentiation requires VDAC1-mediated mitochondrial clearance. Haematologica. 2022;107(1):167–77.

54. Lim ZR, Vassilev S, Leong YW, Hang JW, Renia L, Malleret B, Oh SK. Industrially compatible transfusable iPSC-Derived RBCs: Progress, challenges and prospective solutions. Int J Mol Sci 2021, 22(18).

55. Erb MA, Scott TG, Li BE, Xie H, Paulk J, Seo HS, Souza A, Roberts JM, Dastjerdi S, Buckley DL, et al. Transcription control by the ENL YEATS domain in acute leukaemia. Nature. 2017;543(7644):270–4.

56. Menon V, Ghaffari S. Erythroid enucleation: a gateway into a bloody world. Exp Hematol. 2021;95:13–22.

57. Kobayashi I, Ubukawa K, Sugawara K, Asanuma K, Guo YM, Yamashita J, Takahashi N, Sawada K, Nunomura W. Erythroblast enucleation is a dynein-dependent process. Exp Hematol. 2016;44(4):247–e256210.

58. Huber F, Boire A, Lopez MP, Koenderink GH. Cytoskeletal crosstalk: when three different personalities team up. Curr Opin Cell Biol. 2015;32:39–47.

59. Wang J, Ramirez T, Ji P, Jayapal SR, Lodish HF, Murata-Hori M. Mammalian erythroblast enucleation requires PI3K-dependent cell polarization. J Cell Sci. 2012;125(Pt 2):340–9.

60. Koury ST, Koury MJ, Bondurant MC. Cytoskeletal distribution and function during the maturation and enucleation of mammalian erythroblasts. J Cell Biol. 1989;109(6 Pt 1):3005–13.

61. Tapon N, Hall A. Rho, Rac and Cdc42 GTPases regulate the organization of the actin cytoskeleton. Curr Opin Cell Biol. 1997;9(1):86–92.

62. Konstantinidis DG, Pushkaran S, Johnson JF, Cancelas JA, Manganaris S, Harris CE, Williams DA, Zheng Y, Kalfa TA. Signaling and cytoskeletal requirements in erythroblast enucleation. Blood. 2012;119(25):6118–27.

63. Lammers M, Meyer S, Kuhlmann D, Wittinghofer A. Specificity of interactions between mDia isoforms and rho proteins. J Biol Chem. 2008;283(50):35236–46.

64. Watanabe S, De Zan T, Ishizaki T, Yasuda S, Kamijo H, Yamada D, Aoki T, Kiyonari H, Kaneko H, Shimizu R, et al. Loss of a rho-regulated actin nucleator, mDia2, impairs cytokinesis during mouse fetal erythropoiesis. Cell Rep. 2013;5(4):926–32.

65. Arrindell J, Desnues B. Vimentin: from a cytoskeletal protein to a critical modulator of immune response and a target for infection. Front Immunol. 2023;14:1224352.

66. Jiu Y, Peranen J, Schaible N, Cheng F, Eriksson JE, Krishnan R, Lappalainen P. Vimentin intermediate filaments control actin stress fiber assembly through GEF-H1 and RhoA. J Cell Sci. 2017;130(5):892–902.

67. Krendel M, Zenke FT, Bokoch GM. Nucleotide exchange factor GEF-H1 mediates cross-talk between microtubules and the actin cytoskeleton. Nat Cell Biol. 2002;4(4):294–301.

68. Piekny A, Werner M, Glotzer M. Cytokinesis: welcome to the rho zone. Trends Cell Biol. 2005;15(12):651–8.

69. Ridley AJ. Rho GTPases and actin dynamics in membrane protrusions and vesicle trafficking. Trends Cell Biol. 2006;16(10):522–9.

70. Wheeler AP, Ridley AJ. Why three rho proteins? RhoA, RhoB, RhoC, and cell motility. Exp Cell Res. 2004;301(1):43–9.

71. Hu CK, Coughlin M, Mitchison TJ. Midbody assembly and its regulation during cytokinesis. Mol Biol Cell. 2012;23(6):1024–34.

72. Hiyoshi H, Okada R, Matsuda S, Gotoh K, Akeda Y, Iida T, Kodama T. Interaction between the type III effector VopO and GEF-H1 activates the RhoA-ROCK pathway. PLoS Pathog. 2015;11(3):e1004694.

Publisher's note